

# Advanced Photon Counting Imaging Detectors with 100ps timing for Astronomical and Space Sensing Applications

Oswald Siegmund, John Vallerger, Barry Welsh, Jason McPhate

*Space Sciences Laboratory, U.C. Berkeley*

Mike Rabin, Jeffrey Bloch,

*Los Alamos National Laboratory, NM*

## ABSTRACT

We describe our recent advances in UV-Visible ground and spaceborne detectors that possess the unique ability to record photon X,Y,T high fidelity information. Such sensors have distinct advantages for high speed recording devices for some important time dependent applications in space astronomy. Our most commonly used readout configuration for microchannel plate sensors is the cross delay line anode. We have achieved resolutions of  $< 25 \mu\text{m}$  in tests over  $65 \text{ mm} \times 65 \text{ mm}$  ( $> 2.5\text{k} \times 2.5\text{k}$  resolution elements) with excellent linearity for random photon rates of  $> 1 \text{ MHz}$ , while time tagging events using the MCP output signal to better than 100 ps. Sealed tube (U and visible) microchannel plate cross delay line detectors of this kind have been built and used for observation of flare stars, orbital satellites and space debris using the GALEX satellite. We have also obtained time resolved imaging of the Crab Pulsar with a 1m ground based telescope. To achieve better efficiency, higher counting rate and extended lifetime we are now developing cross strip anode readouts. These have already demonstrated  $5\mu\text{m}$  resolution at  $< 10 \times$  lower gain than the cross delay line readout schemes. High speed electronics for the cross strip are currently under development.

**Keywords:** Microchannel plate, photon counting, imaging, timing

## 1. INTRODUCTION

We have implemented delay line microchannel plate photon counting image readout systems for high-resolution, large format, detectors in spaceborne instrumentation for satellite-based (FUSE[1], GALEX[2], IMAGE[3], SOHO[4], sounding rocket[5], and shuttle payloads (ORFEUS[6]). Many types of scientific observations have been accomplished including stellar, galactic and solar imaging/spectroscopy, aeronomy and the detection of orbital objects. The detector scheme converts incoming source photons to electrons using a photocathode on an entrance window, or by an opaque photocathode deposited onto the first MCP of a stack of MCPs. The MCP stack amplifies the electrons (gain of  $\sim 10^7$ ), depositing the resulting charge onto a delay line readout anode. Delay line schemes encode photon event position centroids by measurement of the difference in arrival time of the event charge at the two ends of a distributed (RC) delay line. The two dimensional delay line configuration is the cross delay line (XDL). The delay-line encoding electronics[7] consists of a fast amplifier for each end of the delay line, followed by constant fraction discriminators (CFDs) and time-to-digital converters (TDC's). Position resolution of delay line anodes is determined by the event timing error. This timing "jitter" is dominated by the constant fraction discriminator (CFD) jitter and walk, and noise in the time-to-amplitude converter (TAC) part of the TDC, which is of the order  $\sim 20 \text{ ps}$  FWHM total in our designs. We have achieved resolutions of  $< 25 \mu\text{m}$  in tests [8] over  $65 \times 65 \text{ mm}$  ( $> 2.5\text{k} \times 2.5\text{k}$  resolution elements). The position linearity is generally better than  $\pm 1$  resolution element over the detector with no signal amplitude dependence of the position resolution over a wide range of MCP gain. In general the multilayer designs are robust, and allow considerable flexibility of design and optimization. With high speed TDC's, we have been able to encode event positions for random photon rates of  $> 1 \text{ MHz}$ , while time tagging events using the MCP output signal to better than 100 ps. Sealed tubes with cross delay line anodes have been built for recording time resolved visible imaging of the Crab Nebula, for the GALEX UV imaging satellite with 65mm active area and for biological fluorescence lifetime imaging[9]. Open face detectors have also been used for photoelectron time resolved spectroscopy at the LBNL ALS synchrotron[10].

## 2. GALEX SATELLITE UV DETECTORS

There have been very few satellite instruments capable of high time resolution imaging in the UV. The Galactic Evolution Explorer (GALEX – NASA (4/2003)) satellite [11], has been accomplishing unprecedented photometric imaging observations of astronomical sources in the near ultraviolet ([NUV] 1750 – 2750Å), and far ultraviolet ([FUV] 1350 – 1750Å). The initial phase of the mission consisted of 5 imaging surveys in each of two bands that cover areas ranging from an all-sky survey (of limiting magnitude  $m_v \sim 21$ ) to an ultra-deep survey that covers only 4 square degrees to a limiting magnitude of  $m_v \sim 26$ . The GALEX instrument is comprised of a 50cm aperture Ritchey-

Chretien UV optimized telescope with a  $1.2^\circ$  field of view and  $\sim 5$  arc-second FWHM resolution imaging. An optical wheel mechanism allows the light-path to be selected for either two-band UV imaging or two-band UV spectroscopy through a dispersive grism. The satellite attitude is dithered in a 1 arcminute spiral for deep targets, while the all-sky survey is obtained by scanning at a rate of 200 arcseconds/sec. Dithering and scanning is performed to average detector non-uniformities and to avoid microchannel plate detector gain fatigue by UV bright stars. The scientific instrument is mounted on a three-axis stabilized spacecraft bus built by Orbital Sciences Corporation (OSC). The satellite was launched via an OSC Pegasus-XL vehicle into a 29 degree inclination, 690 km circular orbit on April 28, 2003. GALEX is also performing low resolution ( $R = 100 - 300$ ) spectroscopic grism sky surveys over the  $1350 - 2800\text{\AA}$  wavelength band. To accomplish high time resolution two dimensional imaging GALEX uses two sealed-tube photon counting detectors of 65mm active area [12, 13] developed at University of California, Berkeley.

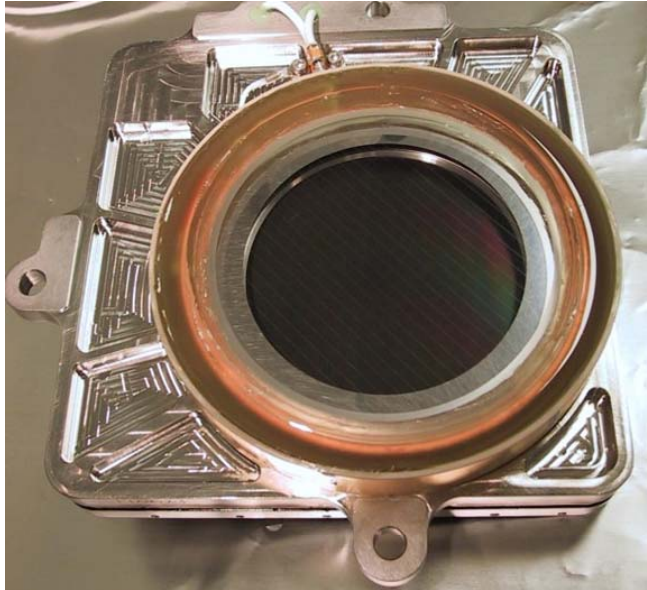


**Fig. 1.** GALEX FUV sealed tube 65mm MCP detector.

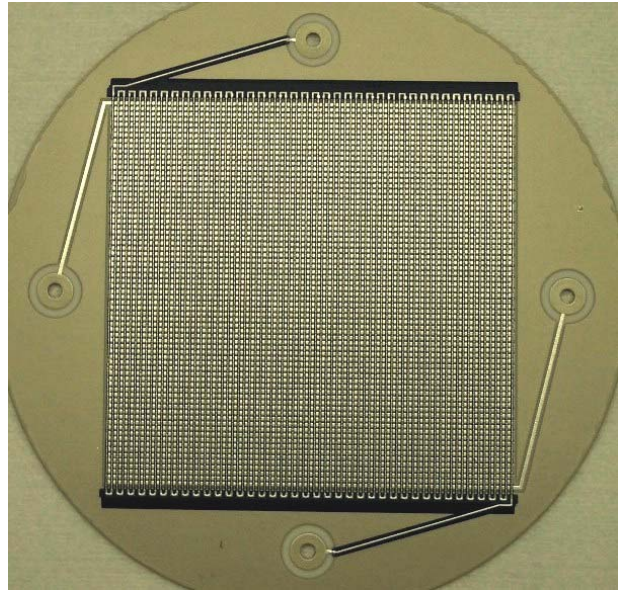


**Fig. 2.** Serpentine 45mm cross delay line ceramic anode.

## 2.1 GALEX Detector Characteristics

GALEX employs two sealed tube detectors, one NUV and one FUV, to achieve its desired wavelength coverage. The detectors are sealed vacuum tube microchannel plate (MCP) detectors with cross delay anode readouts [12,13]. The active area is 65mm diameter ( $4096 \times 4096$  pixel) and is the largest format sealed tube MCP detector currently on orbit. The two detectors are almost identical except for the window material and photocathode chosen for the spectral bandpass. The FUV tube has a  $\text{MgF}_2$  window and a CsI photocathode deposited onto the MCP. The NUV tube has a fused silica window deposited with a semitransparent  $\text{Cs}_2\text{Te}$  photocathode proximity-focused to the MCP. Fig. 1 is a photo of the FUV flight tube. The incident photons pass through the entrance window and interact with the photocathode, resulting in photoelectron emission. The MCP stack multiplies the charge through an electron avalanche with a total gain of about  $10^7$  electrons. This charge cloud is accelerated across a 6 mm gap to the cross delay line (XDL) anode (Fig. 2). The charge is divided equally between the two delay line serpentine electrodes, and the X and Y event positions are determined from the differences in signal arrival time at the two ends of each respective delay serpentine. The delay line detector scheme used is similar to those we have built and successfully flown on the SOHO [14] and IMAGE [15] missions.

The position encoding electronics consist of fast timing amplifiers for the anode signals, followed by time to digital converters (TDC) for each axis. Constant fraction discriminators are used to produce timing signals for each end of the delay line axes, a start from one end, and a stop from the other end which is additionally delayed by a specific length of cable. The time difference between the start and stop signals for each axis are converted to digital positions via a coarse/fine system. A counter is used to determine the number of clock cycles between the start and stop signals to give the 3 most significant bits of the coordinate. Then start and stop interpolators measure the fine position values for each signal relative to the clock. The counter, fine position values, and charge amplitude are then passed to the instrument. The X & Y positions are determined on the ground from the counter and fine position value data. The TDC's, low

voltage power supplies, high voltage power supplies and interface electronics are conglomerated as a Front End Electronics (FEE) stack close to the detectors.

Detector characteristics have been measured in detail [12,13] including the background count rate and distribution, gain, spatial resolution and linearity, flat fields, and quantum efficiency. The resolution and linearity of the tubes was measured at the Space Sciences Laboratory with laboratory electronics before the tubes were sealed. At nominal operating gain of  $\sim 1.5 \times 10^7$  the average full width at half maximum (FWHM) resolution is about  $38 \mu\text{m}$ , as measured with a mask with  $10\mu\text{m}$  pinholes in contact with the first MCP. In both tube types lateral spread of photoelectrons in the window-MCP gap causes some blurring of the resolution. The estimated resolution of the NUV tube with flight electronics is about  $78 \mu\text{m}$  FWHM and the FUV tube with flight electronics is about  $53 \mu\text{m}$  FWHM. The linearity of the detectors in the instrument was also measured at JPL. A calibration mask with  $200 \mu\text{m}$  diameter pinholes was imaged through the GALEX instrument forming images of the pinhole mask on the detector, and this data was used to produce an image correction map. The magnitude of the corrections is  $<200\mu\text{m}$  over the central 50% of the detector area. This is due to the flight electronics non-linearities, but using the derived linearity corrections the image map can be corrected to about 15 microns ( $\sim 1$  arc-second) over about 3/4 of the field of view.

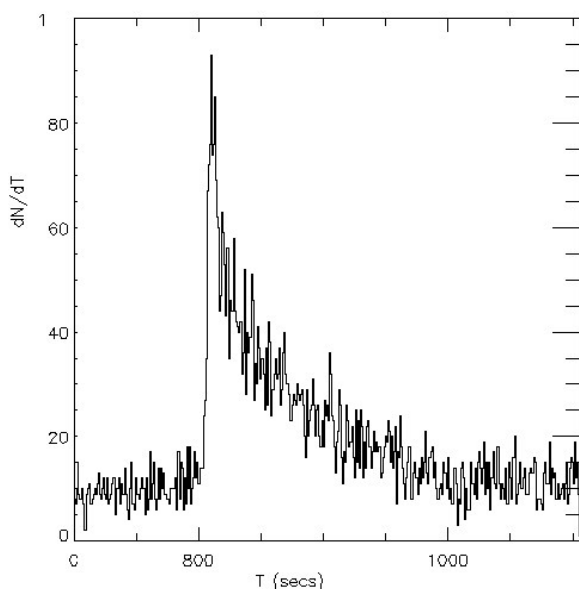


**Fig. 3.** NUV light-curve of a flare on the star SDSS J142551.18+042948.7

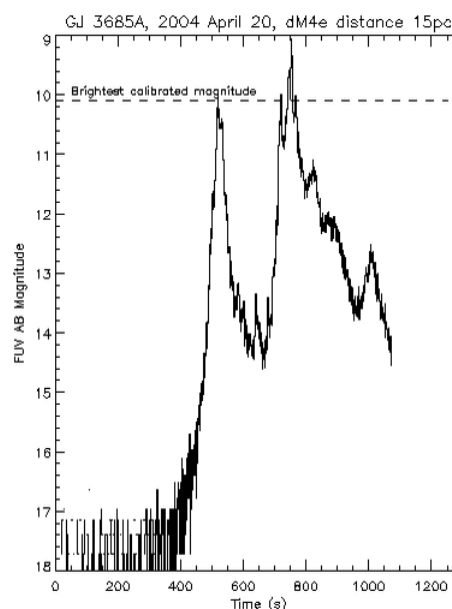


**Fig. 4.** FUV light-curve of the flare on the star GJ 3685A

The QE of the NUV tube (8% @200nm) is typical for  $\text{Cs}_2\text{Te}$  semitransparent photocathodes, and very similar to other MCP-based detectors on orbit, (STIS MAMA on board the Hubble Space Telescope). The QE of the FUV CsI cathode (18% @110nm) is lower than we have achieved on a number of other missions. This was due to deterioration of the photocathode QE during the sealed tube processing, and should be avoidable by process optimization. The overall background in orbit is dominated by sky background, that is zodiacal light (10 kHz) for the NUV detector and diffuse (1 kHz) galactic light for the FUV detector. The counting rate capability of the detector is determined by the global and local rate capabilities. The global electronics processing time is of the order of a few microseconds, so that given the random arrival of photons will experience a 10% event loss at about 20 kHz, which may be easily corrected to establish accurate photometry. The local counting rate limits are different for the FUV and NUV detectors, but are established by the input response to stellar “point” images. The rate at which 10% of the incoming events are lost is  $\sim 97$  events/sec/spot and 420 events/sec/spot for the FUV and NUV detectors respectively. Again it is possible to compensate for the event losses by employing a dead time correction calibration.

## 2.2 High time resolution observations with GALEX

The primary scientific mission of *GALEX* is to carry out imaging sky-surveys in both the NUV and FUV wavelength bands, with the goal of understanding the star formation process in galaxies and how its evolution changes with time (see [11] and references therein). During the course of these sky-survey observations *GALEX* has serendipitously detected numerous variable and transient ultraviolet sources, many of which exhibit much larger flux variations in the

ultraviolet region than those recorded at visible wavelengths. Such stellar sources include M-dwarf flare stars [16], RR Lyrae variable stars [17] and variability associated with the accretion surrounding black holes in active galactic nuclei. The unique capability of UV time-variability studies by *GALEX* is due to the photon counting nature of its detectors, which allow time-tagging of individual UV photons with a precision of  $< 0.05$  seconds. Such timing accuracy *cannot* be obtained with CCD sensors, and in Figs. 3 and 4 we show the UV light-curves of stellar flares. The star GJ 3685A was observed to flare with an overall brightness increase of  $> 4$  magnitudes in both the FUV and NUV bands in a time period of only 20 seconds! Meanwhile, star SDSS J142551.18+042948.7 (Fig. 3) was observed to flare with a rapid onset of  $< 1$  sec.

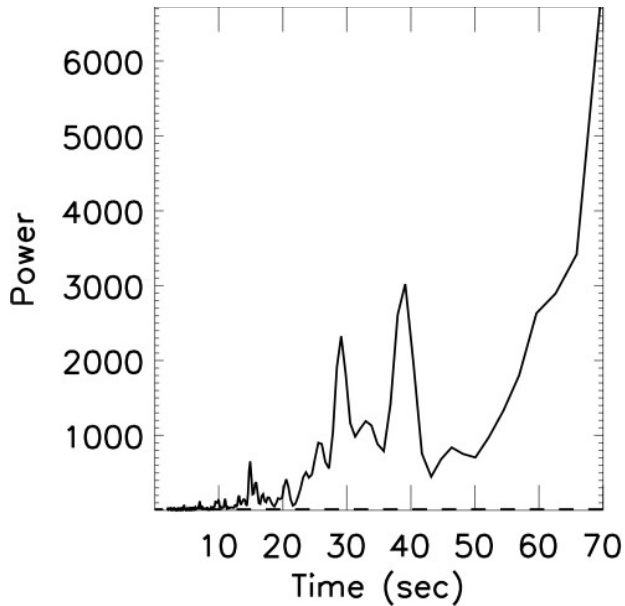


**Fig 5:** Power spectrum of the photon count-rate data for the giant flare on the star GJ 3685A. Oscillations are clearly detected at periods of 30 sec and 40 sec.

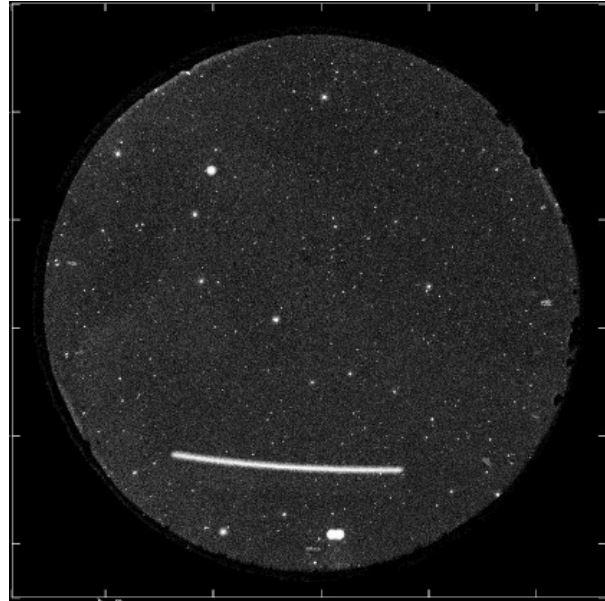


**Fig. 6:** A GALEX image of the track of a bright orbital object as it goes across the field of view.

The time-resolved photon data from these large flare events can be searched for the signatures of magneto-hydrodynamic oscillations that are associated with coronal loops in the active regions on the surface of the flare stars. Such signatures appear as distinct periodicities in the count rate data, which can be revealed by application of Fourier transform techniques. In Fig. 5 we show the result of analysis of the time-tagged flare data for the star GJ 3685A, which clearly reveals two strong peaks (flare oscillation periods of 30 sec and 40 sec) in the power spectrum. These data can then be used to derive the lengths of the coronal loops that are thought to be the cause of the intense stellar flaring [18].

*GALEX* has also serendipitously observed the passage of both asteroids and (presumably) man-made satellites across the  $1.2^\circ$  field-of-view (see Figs. 6 to 8). Such objects are detectable in the UV due to reflection of the incident solar UV flux. Since *GALEX* records high time resolution photon event position information, it is possible to reconstruct images as a function of time, if several orbital parameters such as time of observation and satellite viewing angle are known with precision, then it is possible to determine the orbital path of the observed man-made satellite, or asteroid. The advantages of photon counting devices vs CCDs in accomplishing this task has been discussed in several previous publications [19, 20]. These publications primarily discuss detection in the visible light spectrum, and indicate that photon counting imagers are particularly suited to detection of faint moving objects [20] when using similar (50 cm) optics to that employed by *GALEX*. The detection of such objects by *GALEX* shows that the UV regime may be an advantageous wavelength range to detect such objects due to the inherent extremely low sky-background signal emitted at UV wavelengths. The *GALEX* data have stimulated a growing evaluation of the merits of photon counting sensors for this type of detection, and we have begun to develop techniques to further improve the sensitivity and performance of these devices for various applications.

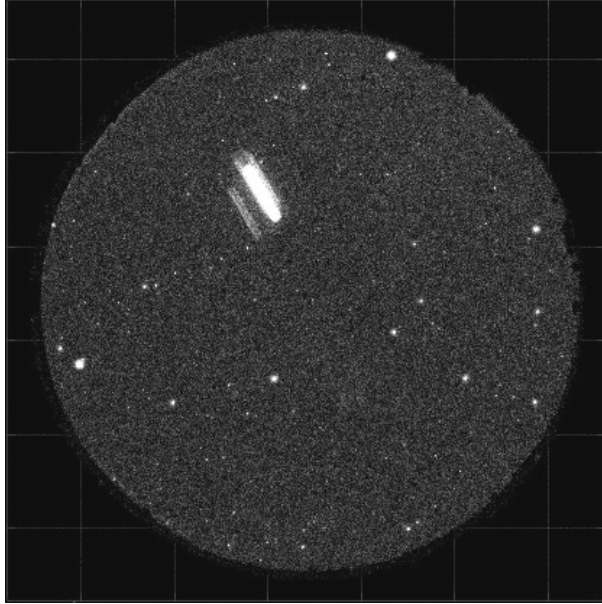


**Fig. 7.** Image of a bright orbital satellite seen while traversing the GALEX field of view (very short integration).

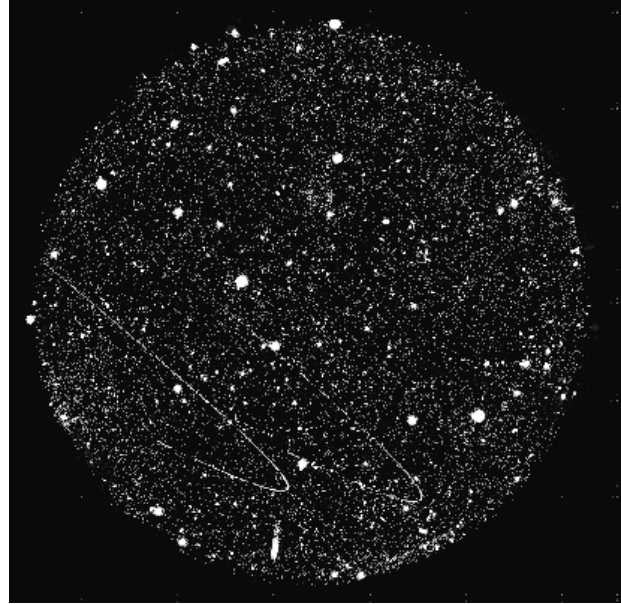


**Fig. 8.** Image of several orbital objects in a longer duration integration showing retrograde motion.

### 3. HIGH TIME RESOLUTION GROUND BASED VISIBLE ASTRONOMY

Celestial sources such as pulsars and white dwarf binaries displaying fast temporal variations ( $< 0.1$  sec) in their emitted high-energy flux, are often associated with the non-thermal particle populations generating X-ray and gamma-ray photons. Photons subsequently emitted at visible wavelengths possess timing and polarization information that is linked these phenomena and can potentially be observed from ground-based telescopes. On time-scales of a tenth of a second, echo mapping of the physical geometry of cataclysmic variable and X-ray binary stars becomes possible, and at the hundredth of a second time-scale direct speckle imaging of nearby stars is achievable. At time-scales of milliseconds the optical emission of pulsars and the detection of the optical analog of kilohertz quasi-periodic oscillations found in X-ray binary accretion disks also becomes feasible. To observe these phenomena with good signal-to-noise and good spatial resolution, a visible wavelength detector that records the arrival time of each emitted photon is required.

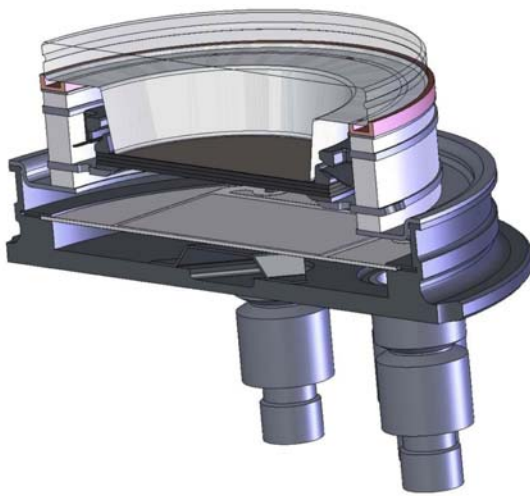


**Fig 9.** Schematic of a sealed tube microchannel plate detector.



**Fig. 10.** 25mm sealed tube cross delay line detector.

We have built several sealed tube devices with 25mm aperture (Figs. 9, 10) that utilize S20 photocathodes deposited onto the input window, a stack of 3 MCPs to amplify the emitted photoelectrons, and cross delay line anodes to record

the photon positions. The QE is typical of S20 cathodes [9], and the spatial linearity is good, but the tubes were not optimized for high position resolution (dominated at  $90\mu\text{m}$  FWHM by the large  $\{600\mu\text{m}\}$  window-MCP proximity gap photoelectron spread). The detector readout is capable of  $\sim 40\mu\text{m}$  FWHM [9] and future devices will employ smaller proximity gaps to achieve this. Events are propagated through the anode in  $\sim 20\text{ns}$ , however the event rate performance is controlled by the electronics chain (amplifiers and TDC) which is capable of processing random events at  $\sim 1\text{ MHz}$ .

Pulsar polarization is an important topic for high time-resolution astronomy. Objects such as the Crab pulsar, with a period of 33ms, require simultaneous measurements of the polarization parameters to determine how the polarization varies across the entire pulsar period. It has been established that a large polarization is associated with the "off" phase of the Crab pulsar's rotational phase. This suggests that the emission during the "off" phase of the visible light-curve is consistent with some form of non-thermal (synchrotron-related) origin. This objective can only be achieved by recording all of the Stokes polarization parameters *for each individual optical pulse*.

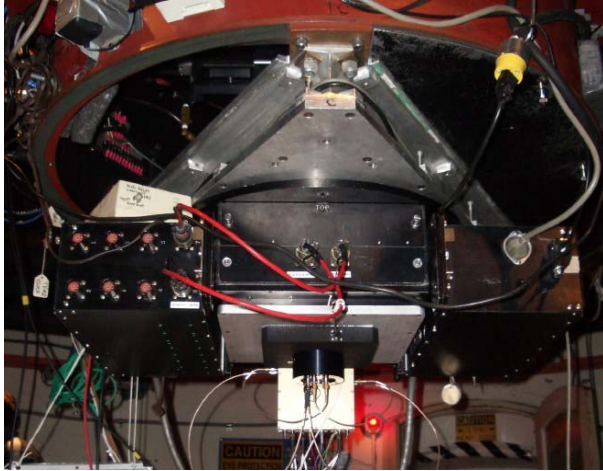


**Fig. 11.** 25mm MCP sealed tube detector mounted at the cassegrain focus of the Lick Observatory Nickel 1m telescope

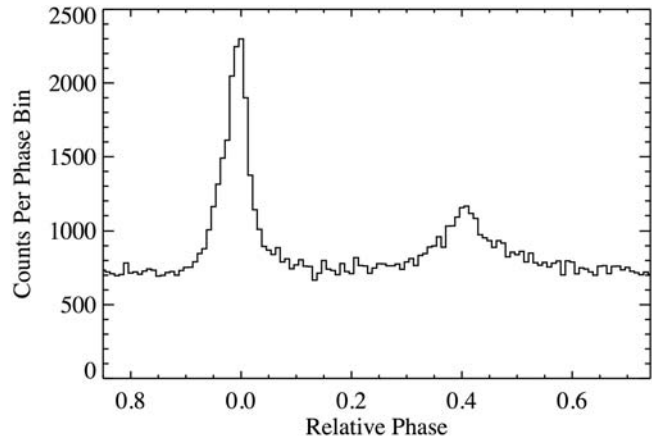


**Fig. 12.** Light curve of the Crab pulsar.  $250\mu\text{s}$  time binning for an 1800 sec exposure time.

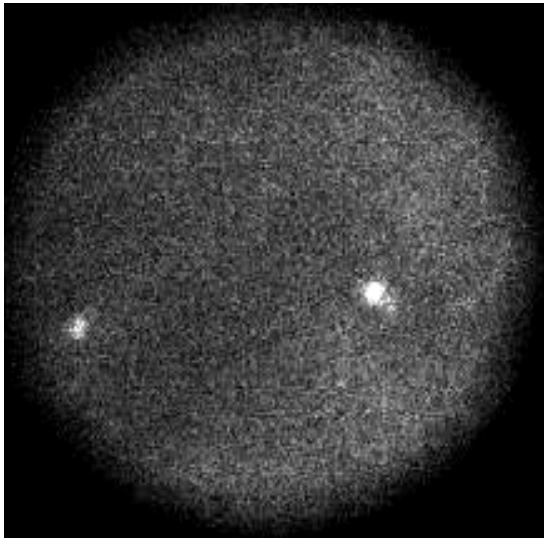


**Fig. 13.** Image of the Crab pulsar at the primary emission peak ( $250\mu\text{s}$  time window).

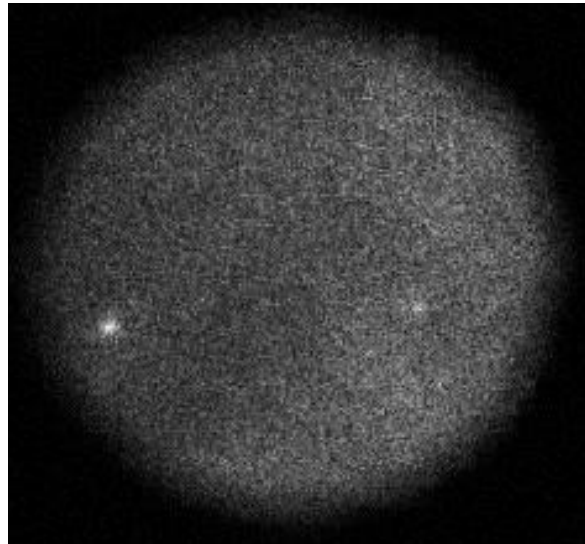


**Fig. 14.** Image of the Crab pulsar at the off phase. ( $250\mu\text{s}$  time window).

To evaluate the possibility of high time resolution pulsar observations a 25mm sealed tube detector system was coupled to the prime focus of the 1m Nickel telescope at Lick Observatory on Mt. Hamilton, CA (<http://mthamilton.ucolick.org>). The TDC provides 25 ns time stamp precision for each photon position recorded and the per event dead time of this TDC is about 400ns, giving  $<30\%$  dead time at 1 Mhz. The TDC time stamp was reset

once per second via a GPS PPS signal, resulting in an absolute timing accuracy of  $\pm 1 \mu\text{s}$ . The tube and amplifiers mounted to an adapter flange at the telescope Cassegrain focus is shown in Fig. 11.

The Crab pulsar was observed on two nights (15 January 2006 and 4 February 2006). Observing conditions were relatively poor on both nights, the seeing was approximately 4–5 arcsec FWHM, and the sky background dominated the detector field. Nevertheless the Crab was clearly visible on our real time display, and we were able to obtain data in a straightforward manner with no accommodations for synchronizing to the Crab period. We observed about 7 to 10 cps from the Crab pulsar, in agreement with our expectations based on source brightness, telescope size, and detector QE. The pulsar light curve shown in Fig. 12 was derived from 1800 seconds of data by extracting the photons that fell within a 3 arcsec radius of the pulsar and making a histogram of their arrival times binned to the expected period of the pulsar for the date of the observation. The characteristic light curve shape [21] for the Crab is clearly visible, and by extracting the photons arriving within any desired time range of the light curve we can produce the corresponding image of the Crab field of view during that time from the stored data set. Images of the Crab extracted from the data set during the primary emission peak and during the quiescent stage are shown in Fig. 13 and 14, and we have also been able to produce a “movie” of the full emission cycle. One of our goals is to employ a polarimeter to project several images of the Crab at different polarizations onto a single detector and obtain the full cycle polarimetric light curves to derive all the Stokes parameters. The recorded data will allow these to be optimally analyzed after the fact, without pre-knowledge of their position, seeing conditions, or pointing constraints. New sealed tubes with higher efficiency (Super GenII, GaAs) cathodes are in development, which in combination with larger telescope apertures will provide the sensitivity necessary to enable these investigations.

#### 4. NEXT GENERATION DETECTOR SYSTEMS

The cross delay line detectors described above have been used for other applications in biological fluorescence lifetime imaging [9] and synchrotron excited photoelectron emission spectroscopy [10]. These uses have demanded the full timing capabilities of our detectors ( $<100\text{ps}$ ) and have required us to adopt a two TDC configuration. Here one TDC is used for X,Y and coarse time stamp, and a second uses the MCP output fast timing signal and a laser, or synchrotron trigger, to provide a fine time tag to 20ps accuracy for each event. Timing resolution is determined by the time jitter of the various components, and we have achieved  $\sim 100\text{ps}$  FWHM (Fig. 15) for both of these applications.

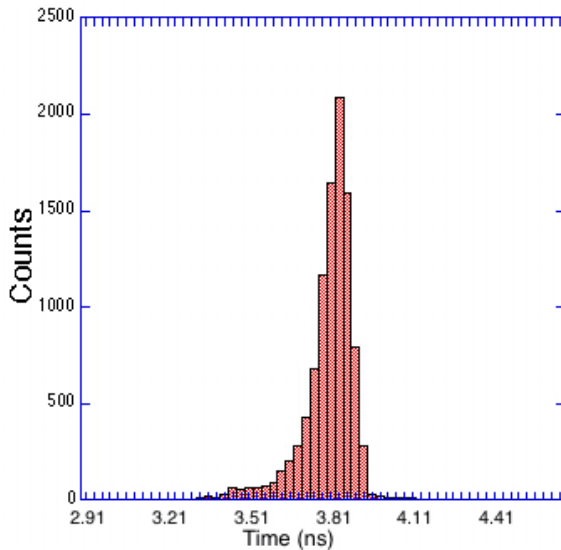


**Fig. 15.** Measured time jitter for a 25mm MCP tube with a 680nm pulsed laser shows  $\sim 100\text{ps}$  FWHM (80ps laser).

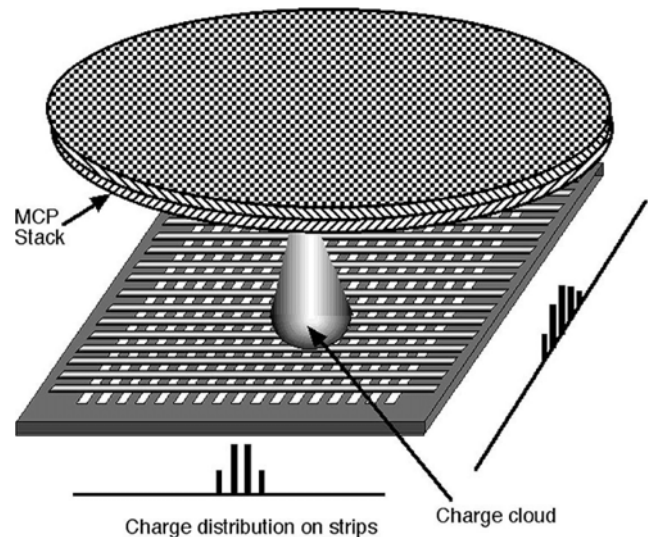


**Fig. 16.** Cross strip anode and MCP functional schematic.

The intrinsic timing performance is sufficient for most of the intended applications, however improvements in spatial resolution, counting rate and lifetime (in high brightness scenarios) are most important for uses such as LIDAR, and in biological fluorescence lifetime imaging. Our goal for the implementation of photon counting MCP sensors is to gain almost two orders of magnitude in throughput while improving the imaging performance and sensitivity by more than factors of four. To achieve these enhancements we are developing the cross strip concept. The cross strip (XS) anode employs many of the physical design techniques used for the XDL anodes. However the XS anode works completely differently than delay-line anodes, to achieve much higher resolution and speed, but at MCP gain several

orders of magnitude lower. The XS anode is a coarse (~0.5 mm) multi-layer metal and ceramic cross strip pattern on an alumina substrate (Fig. 16). On one surface of the substrate the conductors are fabricated as a set of fingers approximately 0.5 mm wide. Then sets of insulating and conducting fingers are applied in the orthogonal direction such that 50 % of the bottom layer is left exposed, while keeping the crosstalk between axes negligible. The top and bottom layers are used to collect the charge from the MCPs with equal charge sharing between the axes. The anodes made in this fashion are low outgassing and accommodate >900°C temperatures, and thus can be put into sealed tube UHV devices. The charge cloud is matched to the anode period so that it is collected on several neighboring fingers to ensure an accurate event centroid can be determined. Each finger of the anode is connected to a charge sensitive amplifier (Fig. 17) and followed by subsequent analog to digital conversion (Fig. 18) of individual strip charge values and a software, or hardware, centroid determination. The center peak of the charge cloud determines the coarse position of the registered photon. The charge cloud centroid ( $\sum nQ_n / \sum Q_n$ ) is calculated with a resolution equivalent to a fraction of the strip width (Q is charge, n is the strip number), which may be accomplished by a hardware or software sum and division. The strip capacitances are small (few pF) and the typical preamplifier noise is <1000 e<sup>-</sup> RMS for signals of a few x 10<sup>5</sup> e<sup>-</sup>. Provided the noise and the number of bits used for signal digitization are sufficient, centroids of better than 1/100 of a strip are possible.

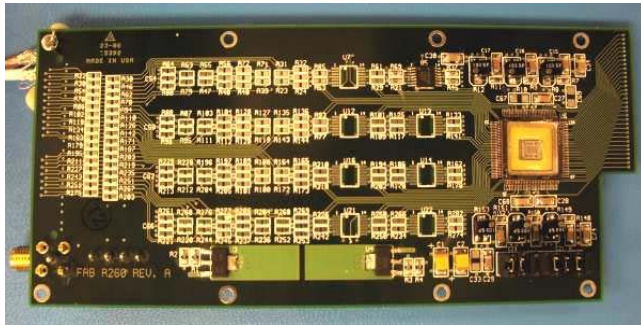


**Fig. 17.** Amplifier board which connects directly to the anode. Uses 2 x 32 parallel channel ASICs (one on each side of the board) and SMT postamplifiers.

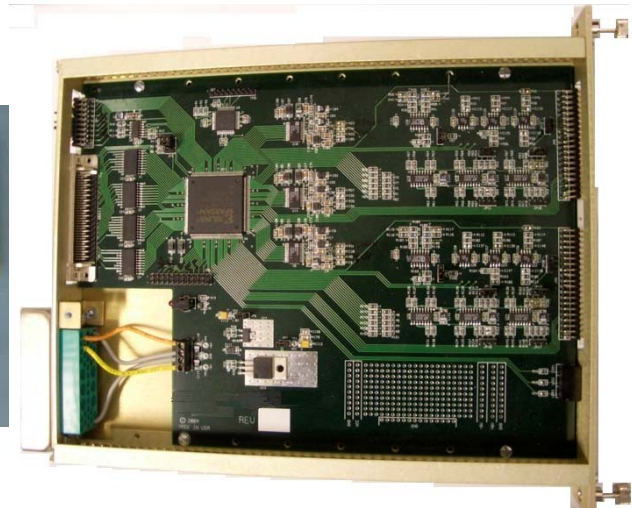


**Fig. 18.** Xilinx based centroid board with serial inputs designed for the IDEAS VaTagP3 amplifier.

A full 32 x 32 mm XS open face laboratory detector has been built and tested extensively, demonstrating excellent resolution (<7 μm FWHM) using low MCP gain (~5 x 10<sup>5</sup>) [22]. The spatial resolution achieved (Fig. 20) is much better than any other existing readout, and can resolve individual MCP pores, and MCP structural defects. XS anodes are mounted ~3 mm behind the MCP's and each strip is connected through a hermetically sealed hole to the backside of the anode, allowing mounting of all the detector electronics outside the vacuum. This allows the amplifier ASIC boards to be easily unplugged/plugged and swapped. The current electronics is relatively slow (<10 kHz) because it is based on a serial readout ASIC amplifier (IDEAS VaTagP3) which has a slow shaping time constant. So we are now developing high speed parallel electronics to digitize the strip signals, and process the events to generate the x, y position with a resolution of <20 μm and time stamp the events with sub-nanosecond accuracy. In the first stage of this development, we are configuring a parallel system using our standard centroiding algorithms which assume a single event at a time on the detector, which should result in rate capabilities of ~ 1 MHz. The next stage of our work will be to improve and speed up the digital filters and algorithms to allow multiple events occur simultaneously on the anode with the goal of a > 5 MHz global throughput. Since the XS anode achieves <7 μm resolution while using low MCP gain (~5 x 10<sup>5</sup>), we can further reduce the gain to ~ 10<sup>5</sup> thus further increasing the MCP local counting rate capacity and overall lifetime of the detector system while achieving acceptable spatial resolution of ~20 μm FWHM.

In the parallel scheme (Fig. 19) each strip on the anode (64 X and 64 Y) is connected directly to a preamp input of a 2 x 32 channel ASIC (RD-20) amplifier board (Fig. 17). The output of these amps are shaped unipolar pulses of ~40 ns rise time, ~160 ns fall time and a conversion gain of 0.72 mV per kilo-electron, with a measured noise of ~800 electrons RMS. The 64 parallel outputs (32 x 2 per axis) are amplified again before being continuously digitized by 64 discrete analog to digital converters operating at >50 mega-samples per second. These digital samples are fed into an FPGA (Xilinx) using a LVDS serial stream of 300MHz bit rate where they are digitally filtered to extract pulse peak information which is then passed to a circuit that uses all 64 channels per axis to derive the event centroid for both X

and Y axes. This centroid position is combined with the digital timing signal. The fine time is generated by the difference between the MCP output pulse from the bottom of the MCP stack and the local FPGA clock while the coarse time is the FPGA clock counter itself sync'ed with an external clock. The events are buffered to await transfer to a downstream computer as an event list of X,Y and T with the appropriate number of bits for the application.

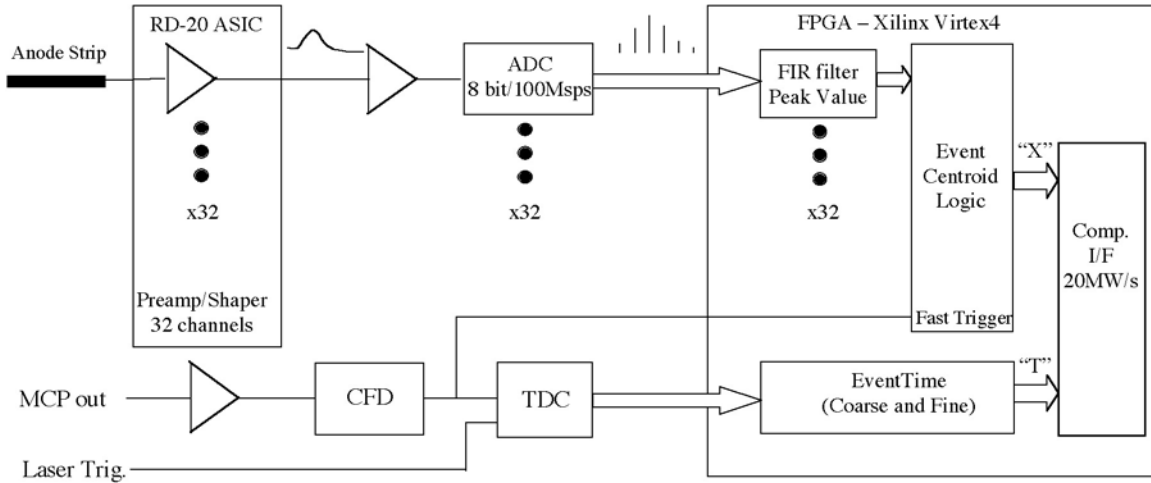


**Fig. 19.** Schematic for a high speed parallel encoding system for XS anodes.

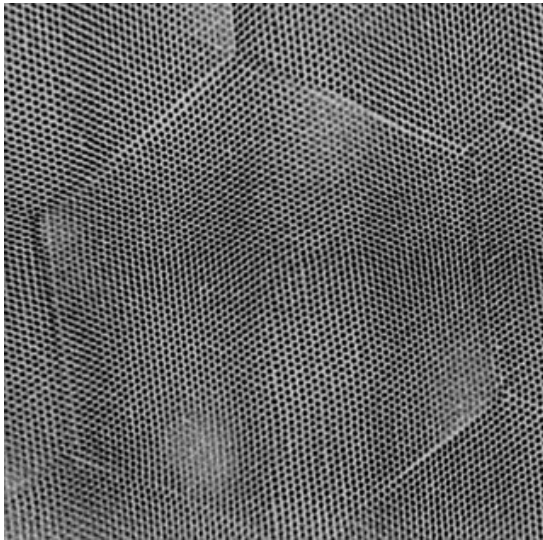


**Fig. 20.** Image of 12  $\mu\text{m}$  MCP pores in a  $1\text{mm}^2$  area using a 32mm XS anode. The MCP multifibers are also visible.

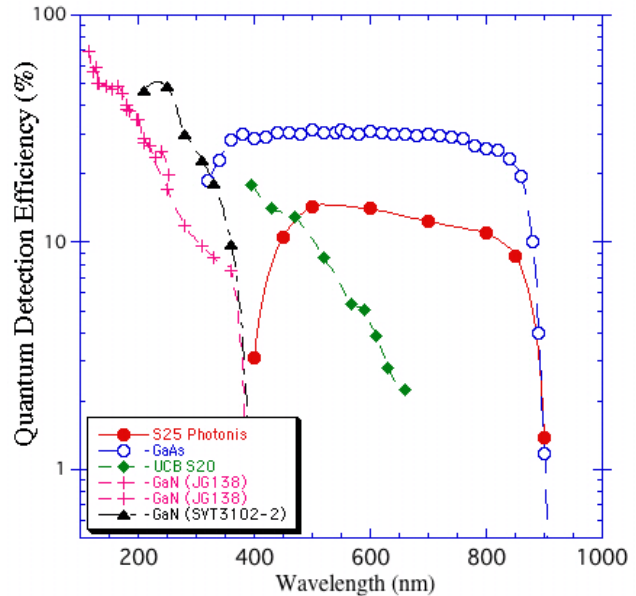


**Fig. 21.** Comparison of photocathodes in the UV and visible regimes. GaN cathodes are under development.

The 32mm XS anode is compatible with a 25mm format sealed tube detector (Fig. 10) and will use a pair of MCPs that will be operated in the range  $10^5$  gain. For initial devices we will employ S20 photocathodes but our intent is to move to extended red SuperGenII photocathodes (S25 Photonis, Fig. 21), and ultimately GaAs photocathodes which will increase the efficiency substantially, obtaining acceptable dark noise for modest cooling ( $-10^\circ\text{C}$ ). In addition we have made significant improvements ( $>50\%$  QE) in development [23] of GaN photocathodes in the ultraviolet regime (see Fig 21). These are also being developed for sealed tubes with the potential to greatly enhance detection efficiency compared with the *GALEX* detectors.

## 6. ACKNOWLEDGEMENTS

GALEX (Galaxy Evolution Explorer) is a NASA Small Explorer, launched in April 2003. We acknowledge the dedicated team of engineers, technicians, and administrative staff from JPL/Caltech, Orbital Sciences Corporation, University of California, Berkeley, Laboratoire Astrophysique Marseille, and the other institutions who made this mission possible. We acknowledge the efforts of J.Hull, J. Malloy, R. Raffanti, X. Michalet, and S. Brown for their work in accomplishing these studies. This work was supported by NSF grant AST0352980, NASA grants NAG5-12710 and NNG05GC79G, and NIH grant 5 R21 RR017474.

## 7. REFERENCES

1. O.H.W. Siegmund, M.A. Gummin, J.M. Stock, et. al, "Performance of the double delay line microchannel plate detect detectors for the Far-Ultraviolet-Spectroscopic Explorer", Proc SPIE 3114, pp.283-94, 1997.
2. O.H.W. Siegmund, P. Jelinsky, S. Jelinsky, et al., "High resolution cross delay line detectors for the GALEX mission", Proc. SPIE 3765, pp.429-40, 1999.
3. J.M. Stock, O.H.W. Siegmund, J.S. Hull, et al., "Cross-delay-line microchannel plate detect detectors for the Spectrographic Imager on the IMAGE satellite", Proc SPIE 3445, pp.407-14, 1998.
4. O.H.W. Siegmund, M.A. Gummin, T. Sasseen, et al., "Microchannel plates for the UVCS and SUMER instruments on the SOHO satellite", Proc. SPIE 2518, pp.334-55, 1995.
5. S. Sarlin, O.H.W. Siegmund, J. Green, "Advanced, two-dimensional, high-resolution microchannel plate solution detector for sounding rocket experiments", Proc. SPIE 2280, pp.46-56, 1994.
6. M. Hurwitz, S. Bowyer. "Ext Extreme UV Astronomy", Pergamon Press, 1991.
7. O.H.W. Siegmund, M.A. Gummin, J.M. Stock et al., "High-resolution monolithic delay-line readout techniques for two-dimensional microchannel plate detectors", Proc SPIE 2006, pp.176-87, 1993.
8. J.V. Vallerger and O.H.W. Siegmund, "2K x 2K resolution element photon counting MCP sensor with >200 kHz event rate capability", Nucl. Instrum. and Meth. in Physics Research, A, 442, p337-341, 2000.
9. O. Siegmund, J. Vallerger, P. Jelinsky, M. Redfern, X. Michalet, S. Weiss, "Cross Delay Line Detectors for High Time Resolution Astronomical Polarimetry and Biological Fluorescence Imaging", IEEE 2005 Nuclear Science Symposium and Medical Imaging Conference, Puerto Rico, October 2005.
10. A.S. Tremsin, G.V. Lebedev, O.H.W. Siegmund, et al, High spatial and temporal resolution photon/electron counting detector for synchrotron radiation research, submitted to Nucl. Instrum. and Meth. A, 2006.
11. D. C. Martin, J. Fanson, D. Schiminovich, et al., "The Galaxy Evolution Explorer: A space ultraviolet survey mission", Astrophysical Journal **619**, pp. L1-L6, 2005.
12. P. Jelinsky, P. Morrissey, James Malloy, S. Jelinsky, and O. Siegmund, C. Martin, D. Schiminovich, K. Forster, T. Wyder & P. Friedman, "Performance Results of the GALEX XDL detectors", Proc. SPIE, **4854**, p.233-240, 2002.
13. O. Siegmund, P. Jelinsky, S. Jelinsky, J. Stock, J. Hull, D. Doliber, J. Zaninovich, A. Tremsin, K. Kromer, "High-resolution cross delay line detectors for the GALEX mission", Proc. SPIE, **3765**, pp. 429-440, 1999.
14. O. H. Siegmund, J. M. Stock, D. R. Marsh, M. A. Gummin, R. Raffanti, J. Hull, Jeffrey, G. A. Gaines, B. Y. Welsh, B. Donakowski, P. N. Jelinsky, T. Sasseen, J. L. Tom, B. Higgins, T. Magoncelli, J. W. Hamilton, S. J. Battel, A. I. Poland, M. D. Jhabvala, K. Sizemore, J. Shannon, "Delay Line Detectors for the UVCS and SUMER Instruments on the SOHO Satellite", Proc. SPIE, **2280**, pp. 89-100, 1994.
15. J. M. Stock, O. H. Siegmund, J. S. Hull, K. E. Kromer, S. R. Jelinsky, H. D. Heetderks, M. L. Lampton, S. B. Mende, "Cross-delay-line microchannel plate detectors for the Spectrographic Imager on the IMAGE satellite" Proc. SPIE, **3445**, 407, 1998.
16. R. D. Robinson, J. M. Wheatley, B. Y. Welsh, et al., "GALEX observations of an energetic ultraviolet flare on the dM4e star GJ 3685A", Astrophysical Journal **633**, pp.447-451, 2005.
17. J. M. Wheatley JM, Welsh BY, Siegmund OHW, et al., "Large-amplitude ultraviolet variations in the RR Lyrae star ROTSE-I J143753.84+345924.8", Astrophysical Journal **619**, pp.L123-L126, 2005.
18. B.Y. Welsh, J. Wheatley, S. Browne, O.H.W. Siegmund et al., "GALEX high time-resolution UV observations of dMe flare events", to appear in Astronomy and Astrophysics, 2006.
19. C. Ho, W. C. Priedhorsky, M. H. Baron, "Detecting small debris using a ground-based photon counting detector", Proc. SPIE **1951**, pp. 67-75, 2003.
20. W. Priedhorsky, J.J. Bloch, "Optical detection of rapidly moving objects in space", Applied Opt. **44** p. 423, 2005.
21. G. Kanbach, S. Kellner, F. Z. Schrey, H. Steinle, C. Straubmeier, H. C. Spruit, "Design and results of the fast timing photopolarimeter OPTIMA", Proc. SPIE **4841**, pp. 82-93, 2003.
22. A. S. Tremsin, O. H. W. Siegmund, J. V. Vallerger, J. Hull, "Cross Strip Readouts for Photon Counting Detectors with High Spatial and Temporal Resolution", IEEE Trans. Nucl. Sci. **51**, pp.1707-1711, 2004.
23. O. Siegmund, J. Vallerger, J. McPhate, J. Malloy, A. Tremsin, A. Martin M. Ulmer, B. Wessels, "Development of GaN photocathodes for UV detectors", Nucl. Instrum. and Meth. A,